NASA Technical Memorandum 86914

Unsteady Pressure Measurements on a Biconvex Airfoil in a Transonic Oscillating Cascade

Loretta M. Shaw, Donald R. Boldman, and Alvin E. Buggele
Lewis Research Center
Cleveland, Ohio

and

Daniel H. Buffum
Purdue University
West Lafayette, Indiana

Prepared for the
Thirtieth International Gas Turbine Conference and Exhibit
sponsored by the American Society of Mechanical Engineers
Houston, Texas, March 17–21, 1985

NASA

UNSTEADY PRESSURE MEASUREMENTS ON A BICONVEX AIRFOIL IN A TRANSONIC OSCILLATING CASCADE

Loretta M. Shaw, Donald R. Boldman, and Alvin E. Buggele
National Aeronautics and Space Administration
Lewis Research Center
Cleveland, Ohio

and

Daniel H. Buffum
Purdue University
West Lafayette, Indiana

E-2408

ABSTRACT

Flush-mounted dynamic pressure transducers were installed on the center airfoil of a transonic oscillating cascade to measure the unsteady aerodynamic response as nine airfoils were simultaneously driven to provide 1.2° of pitching motion about the midchord. Initial tests were performed at an incidence angle of 0.0° and a Mach number of 0.65 in order to obtain results in a shock-free compressible flow field. Subsequent tests were performed at an angle of attack of 7.0° and a Mach number of 0.80 in order to observe the surface pressure response with an oscillating shock near the leading edge of the airfoil. Results are presented for interblade phase angles of 90 and -90° and at blade oscillatory frequencies of 200 and 500 Hz (semi-chord reduced frequencies up to about 0.5 at a Mach number of 0.80). Results from the zero-incidence cascade are compared with a classical unsteady flat-plate analysis. Flow visualization results depicting the shock motion on the airfoils in the high-incidence cascade are discussed. The airfoil pressure data are tabulated.

NOMENCLATURE

C	chord
C_M	unsteady moment coefficient per unit amplitude
C_{M_I}	imaginary part of the unsteady moment coefficient per unit amplitude
C_p	unsteady pressure coefficient per unit amplitude
$\bar{C}_p$	amplitude of unsteady pressure coefficient
$\tilde{C}_p$	time-averaged pressure coefficient, $(P - P_1)/q_1$
C_W	unsteady work done on the system per cycle of oscillation
f	oscillatory frequency
i	incidence angle
$\mathrm{Im}()$	imaginary part of a complex number
M	Mach number
N	airfoil number
p	static pressure
q	dynamic head, $(\gamma/2)pM^2$
$\mathrm{Re}()$	real part of a complex number
S	airfoil spacing
t	time
V	velocity
x_C	coordinate in the chordwise direction
X	nondimensional chordwise direction, x_C/C
X_p	nondimensional position of pitching axis
α	angle of attack
$\bar{\alpha}$	amplitude of airfoil pitching motion
α_0	mean angle of attack
α_R	real part of unsteady pitching motion
β	flow angle
γ	stagger angle
κ	blade angle
ϕ_M	phase lead of unsteady moment coefficient towards motion
ϕ_p	phase lead of unsteady pressure coefficient towards motion

$\phi_{\Delta p}$ phase lead of unsteady pressure difference coefficient towards motion

Ω reduced frequency based on airfoil semi-chord

ω angular frequency

Subscripts:

1 upstream condition

2 downstream condition

U upper or suction surface

L lower or pressure surface

Superscript:

* critical value

INTRODUCTION

This paper addresses the need for aerodynamic data associated with transonic flutter in turbomachinery. Although considerable progress was made in the seventies (1), additional information is needed in order to support the development of contemporary analyses for the prediction of this type of flutter (e.g., (2)). One method of obtaining such information is through the use of a driven linear cascade of the type described in (3).

The previously reported study (3) emphasized the use of flow visualization methods to examine the shock wave dynamics associated with transonic stall flutter. A simple flutter stability model was developed to assess the influence of the direct motion of the oscillating shock on cascade stability. The results in (3) revealed that the shock phase lag, which was measured over a range of reduced frequencies and interblade phase angles was insufficient to imply instability in the cascade based on the simple shock motion model. The present paper represents an extension of the previous work with emphasis on the measurement of the airfoil dynamic surface pressures and subsequent estimates of the cascade stability.

The transonic oscillating cascade used in this investigation was capable of producing realistic reduced frequencies associated with observed transonic stall flutter in turbomachinery while operating at inlet Mach numbers sufficient to provide transonic effects. Driven cascades of this type are usually more complex than classical steady-state cascades because, in addition to meeting the blade-to-blade periodicity requirements in steady-state flow, periodicity must be achieved as the airfoils are driven in a controlled manner (4). In general, the airfoils are oscillated by an external source to provide either a two-dimensional pitching or plunging motion to simulate a torsional or bending mode of flutter. By performing the experiments in this way, the aerodynamic aspects can be separated from the structural aspects of flutter. Various driven cascades are described in (4) to (6).

This paper describes the results of a flutter experiment which was performed with nine driven biconvex airfoils operating in a linear cascade at free stream Mach numbers of 0.65 and 0.80. During the flutter experiments, the airfoils were oscillated to provide a pitching motion of 1.2° about the midchord axis at nominal frequencies of 200 and 500 Hz. The reduced frequency based on the airfoil semichord was about 0.5 at the 500 Hz condition with a free stream Mach number of 0.80. Results from flow visualization experiments are presented for interblade phase angles of $\pm 90°$. The above conditions are believed to be valid for the experimental modeling of the unsteady fluid dynamics associated with torsional stall flutter in fans and compressors.

DESCRIPTION OF CASCADE

Experimental Facility

An overall view of the transonic oscillation cascade is shown in Fig. 1. Room air entered the inlet contraction section and expanded through a 9.78-cm wide by 29.21-cm high test section into a diffuser and exhaust header having a nominal pressure of 3.0 N/cm. Flow rates were controlled by means of two valves located downstream of the diffuser. A partitioned (five section) end-wall boundary layer bleed system located two chord lengths upstream of the airfoils was used to remove the boundary layer on each end wall and provide steady state blade-to-blade periodicity. The bleed passages consisted of perforated plates having an open area ratio of 22.5 percent and a hole diameter of 0.15 cm. The boundary layers on the upper and lower walls of the cascade were removed through slots between the tailboards and the walls. These boundary layer control systems are shown in Fig. 2.

During the flutter experiments the nine airfoils were oscillated in a pitching (torsional) motion about the midchord axes by a mechanical drive system powered by a 100 hp motor. The oscillatory or flutter frequency could be varied in a continuous manner by an eddy-current coupling between the motor and gearbox. The direction of rotation of the motor drive system was reversible so that the sign of the interblade phasing could readily be changed from positive to negative.

Airfoils

Nine two-dimensional, uncambered, biconvex airfoils with a chord of 7.62 cm and a span of 9.6 cm were installed as shown in Fig. 2. The airfoil radius of curvature was 27.4 cm, yielding a maximum thickness of 0.58 cm or a thickness-to-chord ratio of 0.076. This airfoil thickness provided the stiffness required to maintain a two-dimensional flutter mode at the highest frequency of 500 Hz. The airfoils were supported by two trunnions with the centerline located at the midchord as shown in Fig. 3. The larger trunnion which was used to oscillate the airfoil had a diameter of 1.91 cm whereas the freely supported shaft had a diameter of 0.95 cm. Each airfoil and its trunnions were machined from a single piece of titanium containing 6 percent aluminum and 4 percent vanadium.

Test Section

The airfoils were mounted between end walls containing three 0.64-cm-thick mirrors on one side and three optical quality glass windows on the other side (refer to Fig. 2). These mirrors and windows comprised part of a schlieren flow visualization system which was used to observe the flow field. Nonporous bronze alloy bushings containing two "O" rings and helical lubrication grooves were used to support the large trunnion. A similar bronze alloy bushing was lightly pressed into the glass window to provide support for the small trunnion.

The limitation in the region of flow visualization over the airfoil surface was governed by the large trunnion and the size of the corresponding hole in the mirror required to accommodate the small fillet at the airfoil-trunnion junction (Fig. 3). The diameter of this hole, which appears as a shadow in the schlieren images, was 2.3 cm.

$\phi_{\Delta p}$ phase lead of unsteady pressure difference coefficient towards motion

Ω reduced frequency based on airfoil semi-chord

ω angular frequency

Subscripts:

1 upstream condition

2 downstream condition

U upper or suction surface

L lower or pressure surface

Superscript:

* critical value

INTRODUCTION

This paper addresses the need for aerodynamic data associated with transonic flutter in turbomachinery. Although considerable progress was made in the seventies (1), additional information is needed in order to support the development of contemporary analyses for the prediction of this type of flutter (e.g., (2)). One method of obtaining such information is through the use of a driven linear cascade of the type described in (3).

The previously reported study (3) emphasized the use of flow visualization methods to examine the shock wave dynamics associated with transonic stall flutter. A simple flutter stability model was developed to assess the influence of the direct motion of the oscillating shock on cascade stability. The results in (3) revealed that the shock phase lag, which was measured over a range of reduced frequencies and interblade phase angles was insufficient to imply instability in the cascade based on the simple shock motion model. The present paper represents an extension of the previous work with emphasis on the measurement of the airfoil dynamic surface pressures and subsequent estimates of the cascade stability.

The transonic oscillating cascade used in this investigation was capable of producing realistic reduced frequencies associated with observed transonic stall flutter in turbomachinery while operating at inlet Mach numbers sufficient to provide transonic effects. Driven cascades of this type are usually more complex than classical steady-state cascades because, in addition to meeting the blade-to-blade periodicity requirements in steady-state flow, periodicity must be achieved as the airfoils are driven in a controlled manner (4). In general, the airfoils are oscillated by an external source to provide either a two-dimensional pitching or plunging motion to simulate a torsional or bending mode of flutter. By performing the experiments in this way, the aerodynamic aspects can be separated from the structural aspects of flutter. Various driven cascades are described in (4) to (6).

This paper describes the results of a flutter experiment which was performed with nine driven biconvex airfoils operating in a linear cascade at free stream Mach numbers of 0.65 and 0.80. During the flutter experiments, the airfoils were oscillated to provide a pitching motion of 1.2° about the midchord axis at nominal frequencies of 200 and 500 Hz. The reduced frequency based on the airfoil semichord was about 0.5 at the 500 Hz condition with a free stream Mach number of 0.80. Results from flow visualization experiments are presented for interblade phase angles of $\pm 90°$. The above conditions are believed to be valid for the experimental modeling of the unsteady fluid dynamics associated with torsional stall flutter in fans and compressors.

DESCRIPTION OF CASCADE

Experimental Facility

An overall view of the transonic oscillation cascade is shown in Fig. 1. Room air entered the inlet contraction section and expanded through a 9.78-cm wide by 29.21-cm high test section into a diffuser and exhaust header having a nominal pressure of 3.0 N/cm. Flow rates were controlled by means of two valves located downstream of the diffuser. A partitioned (five section) end-wall boundary layer bleed system located two chord lengths upstream of the airfoils was used to remove the boundary layer on each end wall and provide steady state blade-to-blade periodicity. The bleed passages consisted of perforated plates having an open area ratio of 22.5 percent and a hole diameter of 0.15 cm. The boundary layers on the upper and lower walls of the cascade were removed through slots between the tailboards and the walls. These boundary layer control systems are shown in Fig. 2.

During the flutter experiments the nine airfoils were oscillated in a pitching (torsional) motion about the midchord axes by a mechanical drive system powered by a 100 hp motor. The oscillatory or flutter frequency could be varied in a continuous manner by an eddy-current coupling between the motor and gearbox. The direction of rotation of the motor drive system was reversible so that the sign of the interblade phasing could readily be changed from positive to negative.

Airfoils

Nine two-dimensional, uncambered, biconvex airfoils with a chord of 7.62 cm and a span of 9.6 cm were installed as shown in Fig. 2. The airfoil radius of curvature was 27.4 cm, yielding a maximum thickness of 0.58 cm or a thickness-to-chord ratio of 0.076. This airfoil thickness provided the stiffness required to maintain a two-dimensional flutter mode at the highest frequency of 500 Hz. The airfoils were supported by two trunnions with the centerline located at the midchord as shown in Fig. 3. The larger trunnion which was used to oscillate the airfoil had a diameter of 1.91 cm whereas the freely supported shaft had a diameter of 0.95 cm. Each airfoil and its trunnions were machined from a single piece of titanium containing 6 percent aluminum and 4 percent vanadium.

Test Section

The airfoils were mounted between end walls containing three 0.64-cm-thick mirrors on one side and three optical quality glass windows on the other side (refer to Fig. 2). These mirrors and windows comprised part of a schlieren flow visualization system which was used to observe the flow field. Nonporous bronze alloy bushings containing two "O" rings and helical lubrication grooves were used to support the large trunnion. A similar bronze alloy bushing was lightly pressed into the glass window to provide support for the small trunnion.

The limitation in the region of flow visualization over the airfoil surface was governed by the large trunnion and the size of the corresponding hole in the mirror required to accommodate the small fillet at the airfoil-trunnion junction (Fig. 3). The diameter of this hole, which appears as a shadow in the schlieren images, was 2.3 cm.

Airfoil Drive System

A special high-speed mechanical drive system was used to oscillate the airfoils. This system, which represents a modification of the drive mechanism design described in (7), consists of a series of nine barrel cams attached to a common 50-cm diameter shaft. Each cam contained a six-cycle, 1.27-cm-wide by 0.762-cm-deep sinusoidal groove machined in the surface. A close-coupled 7.62-cm long connecting arm and button follower transmitted six cycles of harmonic pitching motion for each revolution of the cam. The amplitude of the airfoil motion was 1.2° as dictated by the cam and follower geometry. Power from the motor drive system was transferred to the cam shaft by a 20.3-cm-wide endless belt consisting of layers of plastic-coated textile fabric, a polyester tension member, and a leather friction surface. The cams and followers were immersed in a multiviscosity 80W-140 high performance gear lubricant to minimize wear. With this system, each flutter test was arbitrarily limited to about 30 sec with 15 to 20 sec at the desired oscillatory frequency. In this operational mode, the cams and button followers incurred negligible wear.

INSTRUMENTATION

Steady-state

The instrumentation included 200 channels of pressures and temperatures from which the steady-state cascade performance was established and an additional 14 channels of high response data for the flutter tests. The steady-state data were recorded through a system of microprocessors coupled to a dedicated minicomputer. The majority of pressures including end wall and airfoil static pressures and boundary layer bleed passage pressures were connected to a scanivalve system containing three 48-channel units scanning in parallel at a rate of seven samples/second. The remainder of the pressures, used as reference values for the scanivalve system and for various traversing probes, were recorded with a system of signal conditioners and pressure transducers. CRT displays were used to expedite tuning of the cascade and provide on-line performance data. Off-line calculations of the detailed performance of the cascade were performed with an IBM 370 computer.

The temperatures in the cascade were essentially equal to the room temperature of 530 °K. These temperatures were measured with chromel-alumel thermocouples.

High Response

The high frequency response measurements included the displacement and frequency of the vibrating airfoils, strain gauge signals on the cam follower arms, and blade surface pressures. Airfoil displacement and oscillatory frequency were measured with an electro-optical displacement meter located outside the test section. This meter tracked a discontinuity of light reflected from the edge of the center airfoil and converted the optical image to an electron image. A servo loop controlled the position of the electron image in an aperture. The deflection current required to keep the image centered in the aperture was a measure of the airfoil angular displacement.

A network of two dual-strain gauges were attached to opposite sides of the arm connecting the airfoil trunnion to the cam. Signals from a conventional full bridge circuit were recorded in order to determine the dynamic phase differences between the oscillating airfoils and verify the interblade phase angle which was preset by manually rotating each of the cams on the cam shaft.

The center airfoil in the cascade contained six commercial high-response strain-isolated pressure transducers which were mounted with the sensing elements aligned flush with the airfoil surface as shown in Fig. 4. The leads from the transducers were routed through the large trunnion by means of slots machined in the opposite surface of the airfoil. The transducers were a modified commercial type having a silicon diaphragm. The selection of the transducer and mounting arrangement was based on the results described in (8) in conjunction with in-house studies of various installation configurations designed to minimize the effects of strain-induced apparent pressure response. The transducer was a 69 kPa cylindrical type which was modified by reducing the overall length and mounted as shown in (8), configuration "E". The signals were amplified in the test cell close to the source followed by a second stage of amplification in the adjacent control room to achieve the maximum dynamic range compatible with the recording system.

All high response measurements were recorded on a frequency modulated (FM) magnetic tape recorder with a frequency response of 10 kHz. The output from the taped signals were analyzed on a Fast Fourier Transform (FFT) analyzer.

Flow visualization was accomplished by means of a double-pass schlieren system shown in Fig. 5. The schlieren images were photographed with a 16-mm high speed motion picture camera operating at about 5000 frames/second (or about 10 frames/cycle of airfoil motion).

The periodicity in the cascade was determined by the uniformity of rows of upstream and downstream static pressures along the length of the cascade. The pressure taps were spaced 2.92 cm apart (1/2 of the blade spacing) and were one and two chord lengths upstream and downstream of the airfoils, respectively.

Flow angle probes were located at three tangential positions upstream of the airfoils for measuring the inlet flow angle and flow uniformity in the tangential direction. These measurements were obtained in the plane of the static pressure taps. The location of the upstream probes is shown schematically in Fig. 6.

GEOMETRIC PARAMETERS

The coordinate system and geometric parameters for the cascade are shown in Fig. 6. All of the tests were performed at inlet flow angles, β_1, of 53° and 60° which provided angles of attack, α_0, of 0.0° and 7.0°, respectively. The blade stagger angle, γ, was fixed at 53°. The solidity or chord-to-spacing ratio, C/S, was 1.3. Since the biconvex airfoils were uncambered, $i = \alpha_0$ and $\gamma = \kappa_1 = \kappa_2$.

RESULTS

Details of the steady-state flow field have already been presented in (3) and, therefore, will not be repeated herein. The principal goal of this experiment was to measure and assess the airfoil unsteady surface pressures. Consequently, the pressure data will be discussed along with cascade stability results as determined from the integrated pressure distributions. The pressure data will be presented in tabular form in order to serve as a potential aid to the development of new computational methods for the prediction of flutter instability. Comparisons of the experimental results with predictions based on a flat-plate calculation method will be made as appropriate.

Steady-state Airfoil Pressure Distributions

The chordwise distributions of time-averaged pressure coefficient, $\bar{C}_p$, on the center airfoil are shown in Fig. 7 for Mach numbers of 0.65 ($\alpha_0 = 0.0^\circ$) and 0.80 ($\alpha_0 = 7.0^\circ$) and are tabulated in Table I. The results for $\alpha_0 = 0.0^\circ$ show an appreciable asymmetry in the distributions resulting from the influence of the staggered cascade. At a Mach number of 0.80 and corresponding angle of attack of 7.0°, the distributions reveal the presence of transonic flow (region above $\bar{C}_p^*$) and the pronounced rise in pressure resulting from the formation of a lambda-type shock wave. This region of supersonic flow extends over a distance of about 10 percent of the chord as shown in Fig. 7.

Tests with Oscillating Airfoils

The airfoils were oscillated in simple harmonic motion to provide information on the phase between the unsteady moment and airfoil motion. This motion can be described by the following equation:

$$\alpha(t) = \alpha_0 - \bar{\alpha} \cos \omega t \qquad (1)$$

where the amplitude, $\bar{\alpha}$, was 1.2° and the mean angle of attack, α_0, was either 0.0° or 7.0°. The airfoils were oscillated at 200 and 500 Hz which yielded reduced frequencies ranging from 0.18 to 0.46 at a Mach number of 0.80 where the reduced frequency is

$$\Omega = \frac{\omega C}{2V_1} \qquad (2)$$

The results were obtained for interblade phase angles of 90° and -90°. Positive interblade phase angle is defined such that airfoil N leads airfoil N + 1, etc. (refer to Fig. 6). Positive interblade phase angles would correspond to a wave moving in the direction of rotor rotation.

In order to measure the pressures on the suction and pressure surfaces, it was necessary to rotate the center airfoil 180° and perform the tests in two steps. The symmetry of the biconvex airfoil permitted this type of data acquisition at the expense of doubling the number of tests relative to an experiment in which both surfaces of the airfoil are instrumented with pressure transducers (or two airfoils are instrumented to acquire the measurements in a single blade passage). The pressure data was reduced by the procedure given in the Appendix to yield local values of the moment coefficient. Subsequent integration of the chordwise distribution of moment coefficient yielded the aerodynamic damping, Ξ, where

$$\Xi = -C_{M_I} \qquad (3)$$

Therefore for negative values of the imaginary part of the moment coefficient, the aerodynamic damping is positive, i.e., the cascade is stable.

Unsteady Aerodynamic Response

Chordwise distributions of aerodynamic phase angle, $\phi_{\Delta p}$, and pressure difference coefficient, $\Delta\bar{C}_p$, are presented in Fig. 8 for a Mach Number of 0.65 and an angle of attack of 0.0°. The phase angle is relatively constant over the first 60 percent of the chord for both of the interblade phase angles and frequencies as shown in Fig. 8(a). The level of the phase angle distribution for the 500 Hz run at an interblade phase angle of 90° is noticeably lower than the levels for the other three test conditions. In this case the pressure lagged the motion by nearly 150° over much of the airfoil whereas in the other cases it lead the motion by a few degrees.

The pressure distributions shown in Fig. 8(b) are generally well-behaved with the exception of the 500 Hz results at an interblade phase angle of 90°, which as noted above, exhibited much higher values of aerodynamic phase lag than observed at the other conditions. Here the pressure difference coefficient increased appreciably over the first 25 percent of the airfoil and then attained a level over the midchord region that was similar to the 500 Hz data with an interblade phase angle of -90°.

The unsteady response data for each surface of the airfoil from which the results in Fig. 8 were derived are tabulated in Tables II(a) to II(d).

The response data for a Mach number of 0.80 and an angle of attack of 7.0° are presented in Fig. 9. The data exhibit a nearly constant level of aerodynamic phase angle over most of the chord (Fig. 9(a)). The phase angles were generally positive and less than 90°, i.e., the pressure response generally leads the blade motion by less than 90°.

The distributions of unsteady pressure difference coefficients are presented in Fig. 9(b). The results are well organized and similar to the results in Fig. 8 which were obtained at a Mach number of 0.65 and at an angle of attack of 0.0°. The presence of the shock wave near the leading edge of the suction surface did not manifest itself in an obvious way through differences in the local values of $\Delta\bar{C}_p$.

The unsteady response data for each surface of the airfoil from which the results in Fig. 9 were derived are tabulated in Tables II(e) to II(h).

Cascade Stability

The stability of the cascade was determined by computing the imaginary part of the moment coefficient C_{M_I} (Eq. (3)) from the pressure difference distributions shown in Figs. 8 and 9. The distributions were closed at the leading and trailing edges of the airfoil by assuming a constant level of $\Delta\bar{C}_p$ as in (5).

The results for $M_1 = 0.65$ and $\alpha_0 = 0.0^\circ$ are shown in Fig. 10. Instability occurred at one of the four experimental conditions; namely, at an interblade phase angle of 90° and a frequency of 200 Hz ($\Omega = 0.221$). These results are consistent with predictions based on a flat-plate analysis (9) although the observed levels of C_{M_I} are somewhat higher than flat-plate theory.

The results for $M_1 = 0.80$ and $\alpha_0 = 7.0^\circ$ are shown in Fig. 11. As in the previous case, instability was observed at an interblade phase angle of 90° and at a frequency of 200 Hz ($\Omega = 0.185$). All of the other experimental cases exhibited stability.

Flow Visualization

Individual frames from the high speed movies of schlieren images of the flow were reprooduced in a 35 mm format and are shown in Fig. 12. These pictures represent one state of the flow during a cycle of oscillation at a Mach number of 0.80. The most pronounced feature is a total separation of the flow downstream of the shock as the blade pitches upward towards the maximum angle of attack of 8.2°. This separation was not evident while operating at steady-state conditions and was not evident in the previous study (3) at the same conditions. It is believed that this total separation became apparent in these latest tests because of an improved optical system which permitted a better cutoff at the knife edge in the schlieren system (Fig. 5). The separation was repeatable from blade to blade

within the visible flow field which encompassed approximately the three central airfoils.

DISCUSSION

Results of unsteady aerodynamic response have been presented for two cascade conditions; namely, a 0° angle of attack cascade operating at an inlet Mach number of 0.65 and the same cascade operating at an angle of attack of 7.0° and a corresponding inlet Mach number of 0.80. In the latter case, a lambda-type shock wave was present near the leading edge of the suction surface of the airfoils. The tests were performed at interblade phase angles of $\pm 90^\circ$ in order to explore conditions which might yield high levels of stability and instability. These conditions were selected on the basis of results from a flat-plate analysis. The unsteady aerodynamic data were obtained from six high-response pressure transducers mounted flush with the surface of the center airfoil.

It was anticipated that the cascade stability results at the zero angle of attack condition and a Mach number of 0.65 would be in reasonable agreement with flat-plate theory since the surface pressure gradients on the biconvex airfoils were low. The stability results indeed corroborated this hypothesis. However it was somewhat surprising to discover that the results for the more ambitious case in which the angle of attack was 7.0° and the inlet Mach number was 0.80 were quite similar to the flat-plate results. It is recognized that the uncertainty in the stability results for the transonic flow experiment is greater than for the subsonic flow experiment because of a limitation in the number of transducers used to acquire the pressure data. The six chordwise transducers, which were considered to be the maximum allowable number for structural reasons, would not be expected to present problems at the zero angle of attack flow condition but could be marginal at an angle of attack of 7.0° where the local pressure gradient would be large due to the presence of a shock wave near the leading edge. This factor should be considered in interpreting the stability results for the high Mach number cascade flow. Because of the limitations in chordwise resolution of the unsteady pressures, especially at the high Mach number condition, the pressure data are presented in tabular form. Consequently, comparisons of theory with experiment can be made on the basis of both the individual pressures and the calculated stability.

REFERENCES

1. Sisto, F., "Overview: NASA/AF/NAVY Symposium on Aeroelasticity of Turbine Engines," ME-RT-81003, Stevens Institute of Technology, Hoboken, N.J., Oct. 1980.
2. Verdon, Joseph M., and Caspar, Joseph R., "A Linear Aerodynamic Analysis for Unsteady Transonic Cascades," NASA CR-3833, 1984.
3. Boldman, D.R., Buggele, A.E., and Michalson, G.M., "Stall Flutter Experiment in a Transonic Oscillating Linear Cascade," NASA TM-82655, 1981.
4. Carta, F.O., "An Experimental Investigation of Gapwise Periodicity and Unsteady Aerodynamic Response in an Oscillating Cascade, Part I: Experimental and Theoretical Results," NASA CR-3513, 1982.
5. Riffel, R.E., and Rothrock, M.D., "Experimental Determination of Unsteady Blade Element Aerodynamics in Cascades, Vol. 1: Torsional Mode Cascade," EDR-10119-Vol. 1, Detroit Diesel Allison, Indianapolis, IN, June 1980. (NASA CR-159831)
6. Szchenyi, E., and Finas, R., "Aeroelasticity Testing in a Straight Cascade Wind Tunnel," Aeroelasticity in Turbomachines, Office National d'Etudes et de Recherches Aerospatiales (ONERA), Lausanne, Switzerland, 1980.
7. Boldman, D.R., and Buggele, A.E., "Wind Tunnel Tests of a Blade Subjected to Midchord Torsional Oscillation at High Subsonic Stall Flutter Conditions," NASA TM-78998, 1978.
8. Grant, H.P., and Lanati, G.A., "Instrumentation for Measuring the Dynamic Pressure on Rotating Compressor Blades," PWA-5558-12, United Technologies Corporation, East Hartford, CT, Sept. 1978. (NASA CR-159466)
9. Smith, S.N., "Discrete Frequency Sound Generation in Axial Flow Turbomachines," ARC-R/M-3709, Aeronautical Research Council, London, England, 1973.

APPENDIX - CALCULATION OF CASCADE STABILITY FROM UNSTEADY SURFACE PRESSURE MEASUREMENTS

Signals from the high response pressure transducers on the center airfoil were tape recorded and analyzed on a Fast-Fourier Transform analyzer to provide the amplitude of the first harmonic component of pressure and its phase relative to the blade motion signal. The pressure signals were converted to coefficient form as in (4) such that

$$C_p(X,t) = \frac{p(X,t)}{q_1 \bar{\alpha}} = \bar{C}_p(X)\, e^{i(\omega t + \phi_p)} \tag{A1}$$

where ϕ_p is the phase by which the pressure leads the airfoil motion and $X = x_c/C$.

The airfoil motion can be expressed as

$$\alpha(t) = \alpha_0 + \bar{\alpha}\, e^{i\omega t} \tag{A2}$$

where α_0 is either 0.0° or 7.0° and $\bar{\alpha}$ is 1.2°. The pressure difference across the airfoil is defined in coefficient form as

$$\Delta C_p(X,t) = C_{p_L}(X,t) - C_{p_U}(X,t) = \Delta \bar{C}_p(X)\, e^{i(\omega t + \phi_{\Delta p})} \tag{A3}$$

The unsteady moment is

$$C_M(t) = \int_0^1 (X_p - X)\Delta C_p(X,t)\,dx = \bar{C}_M\, e^{i(\omega t + \phi_M)} \tag{A4}$$

where X_p is the nondimensional position of the pitching axis from the leading edge of the airfoil. The value of X_p in this study was 0.5.

The unsteady work per cycle is defined as

$$C_W = \oint \mathrm{Re}\left\{\bar{\alpha}\, C_M(t)\right\} d\alpha_R \tag{A5}$$

Upon substituting from Eqs. (A2) and (A4) and integrating Eq. (A5), the unsteady work per cycle can be expressed as

$$C_W = \pi \bar{\alpha}^2 \bar{C}_M \sin \phi_M = \pi \bar{\alpha}^2 C_{M_I} \tag{A6}$$

A positive value of C_W implies the airstream is doing work on the airfoil, i.e., negative damping takes place and the airfoil is unstable. The aerodynamic damping is given by

$$\Xi = -\frac{C_W}{\pi\bar{\alpha}^2} = -C_{M_I} \tag{A7}$$

The stability results in the present paper are presented in terms of C_{M_I}; therefore positive values of C_{M_I} imply negative damping or instability.

TABLE I. - TIME AVERAGED SURFACE PRESSURES ON CENTER AIRFOIL

(a) $M_1 = 0.65$, $\alpha_o = 0°$, $P_1 = 75.54$ kPa, $q_1 = 22.04$ kPa

X_c/C	$\bar{C}p_L$	$\bar{C}p_U$
0.016	-0.026	-0.100
.033	-.064	-.044
.050	-.099	-.052
.067	-.139	-.073
.083	-.168	-.075
.100	-.178	-.064
.117	-.193	-.064
.183	-.270	-.069
.333	-.374	-.099
.500	-.389	------
.667	-.249	-.229
.817	-.219	-.215
.983	-.066	-.063

(b) $M_1 = 0.80$, $\alpha_o = 7°$, $P_1 = 64.09$ kPa, $q_1 = 28.72$ kPa

0.016	0.761	-1.156
.033	.617	-1.233
.050	.522	-1.029
.067	.437	-.781
.083	.369	-.413
.100	.321	-.230
.177	.277	-.230
.183	.168	-.163
.333	.055	-.015
.500	.023	------
.667	.109	.097
.817	.105	.165
.983	.289	.260

TABLE II. - UNSTEADY SURFACE PRESSURES ON CENTER AIRFOIL

(a) $M_1 = 0.65$, $\alpha_0 = 0^\circ$, $f = 200$ Hz, $\sigma = 90^\circ$, $p = 73.91$ kPa

	Suction surface			Pressure surface		
x_c/C	$\bar{C}_p$	ReC_p	ImC_p	$\bar{C}_p$	ReC_p	ImC_p
0.12	5.566	-5.565	-0.097	4.115	2.088	3.546
.25	3.730	-3.725	-.182	3.898	.292	3.887
.40	2.451	-2.276	.910	3.872	1.830	3.412
.60	3.698	-2.432	2.788	2.267	.640	2.175
.75	2.427	.212	2.418	.472	.247	.402
.88	2.984	-.073	2.983	3.934	-2.427	3.096

(b) $M_1 = 0.65$, $\alpha_0 = 0^\circ$, $f = 500$ Hz, $\sigma = 90^\circ$, $p = 74.19$ kPa

0.12	6.935	1.073	6.851	8.144	0.046	8.132
.25	5.220	3.842	3.533	8.977	-6.264	-6.430
.40	3.902	2.091	3.294	11.473	-2.111	11.277
.60	4.377	3.692	2.352	9.429	-.740	9.399
.75	7.298	4.652	5.623	3.270	-3.125	.962
.88	6.358	5.484	3.218	10.195	-7.876	6.423

(c) $M_1 = 0.65$, $\alpha_0 = 0^\circ$, $f = 200$ Hz, $\sigma = -90^\circ$, $p = 74.19$ kPa

0.12	4.929	-4.478	2.060	3.611	2.758	-2.331
.25	3.762	-3.753	-2.690	1.761	1.878	-.655
.40	3.447	-3.187	-1.316	3.176	2.842	-1.417
.60	5.601	-4.946	-2.630	1.031	1.181	-5.760
.75	5.532	-2.989	-4.655	.428	.290	-.314
.88	3.448	-.776	-3.360	1.828	.204	1.816

(d) $M_1 = 0.65$, $\alpha_0 = 0^\circ$, $f = 500$ Hz, $\sigma = -90^\circ$, $p = 74.17$ kPa

0.12	4.731	-2.847	3.778	7.186	7.974	-3.458
.25	5.253	-5.248	.220	5.432	5.429	.190
.40	1.611	-1.111	-1.167	5.961	6.868	-1.137
.60	7.355	-6.258	-3.865	2.977	2.687	1.282
.75	-----	------	------	2.224	2.220	-.136
.88	4.341	-1.463	-4.086	2.867	2.662	1.065

(e) $M_1 = 0.80$, $\alpha_0 = 7^\circ$, $f = 200$ Hz, $\sigma = 90^\circ$, $p = 64.29$ kPa

0.12	5.003	-4.888	1.066	5.824	4.906	3.138
.25	3.684	-3.449	1.296	4.445	2.904	3.365
.40	2.675	-2.053	1.716	3.450	1.588	3.063
.60	3.050	-1.998	2.306	2.418	.642	2.331
.75	3.368	-2.398	2.365	.571	.223	.526
.88	2.581	-1.853	1.796	3.326	1.326	3.050

(f) $M_1 = 0.80$, $\alpha_0 = 7^\circ$, $f = 500$ Hz, $\sigma = 90^\circ$, $p = 64.38$ kPa

0.12	6.473	-1.013	6.393	10.338	10.311	-.739
.25	4.847	-1.057	4.731	3.232	1.863	-2.641
.40	5.781	.914	5.708	1.062	9.439	4.872
.60	4.999	-2.704	4.992	8.030	5.456	5.892
.75	9.315	-.698	9.289	2.603	2.155	1.459
.88	5.597	-.283	5.590	3.300	-1.003	3.144

(g) $M_1 = 0.80$, $\alpha_0 = 7^\circ$, $f = 200$ Hz, $\sigma = -90^\circ$, $p = 64.56$ kPa

0.12	4.368	-3.356	2.796	5.744	4.173	-3.946
.25	3.835	-3.658	1.153	3.480	2.434	-2.486
.40	3.450	-3.432	-3.486	2.089	1.762	-1.122
.60	4.161	-4.050	-.957	.645	.556	-.329
.75	3.851	-3.694	-1.087	.237	.219	-.090
.88	2.247	-1.231	-1.881	3.626	2.287	-2.814

(h) $M_1 = 0.80$, $\alpha_0 = 7^\circ$, $f = 500$ Hz, $\sigma = -90^\circ$, $p = 64.61$ kPa

0.12	5.461	-4.666	2.837	8.853	5.583	-6.870
.25	5.869	-5.805	-.868	2.806	1.613	-2.296
.40	3.023	-2.369	-1.878	4.583	4.449	-1.101
.60	5.816	-4.436	-3.762	1.141	1.619	1.149
.75	5.753	-3.454	-4.600	1.385	1.385	-4.836
.88	3.123	.286	-3.160	4.716	-1.101	-4.585

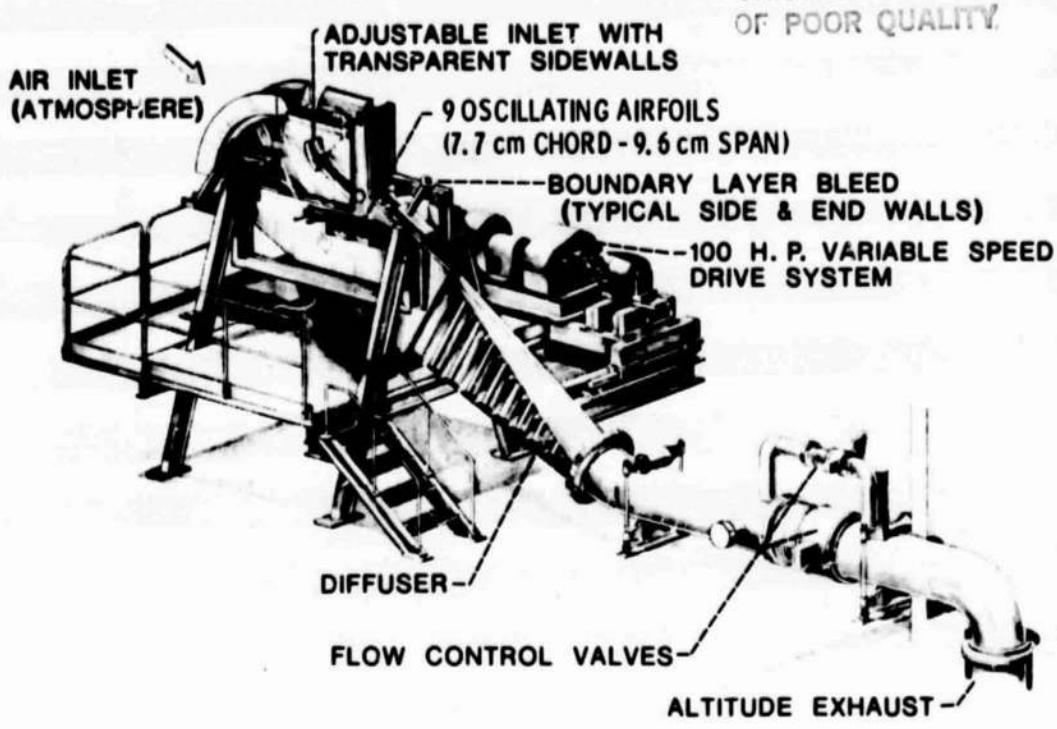

Figure 1. - Transonic oscillating cascade.

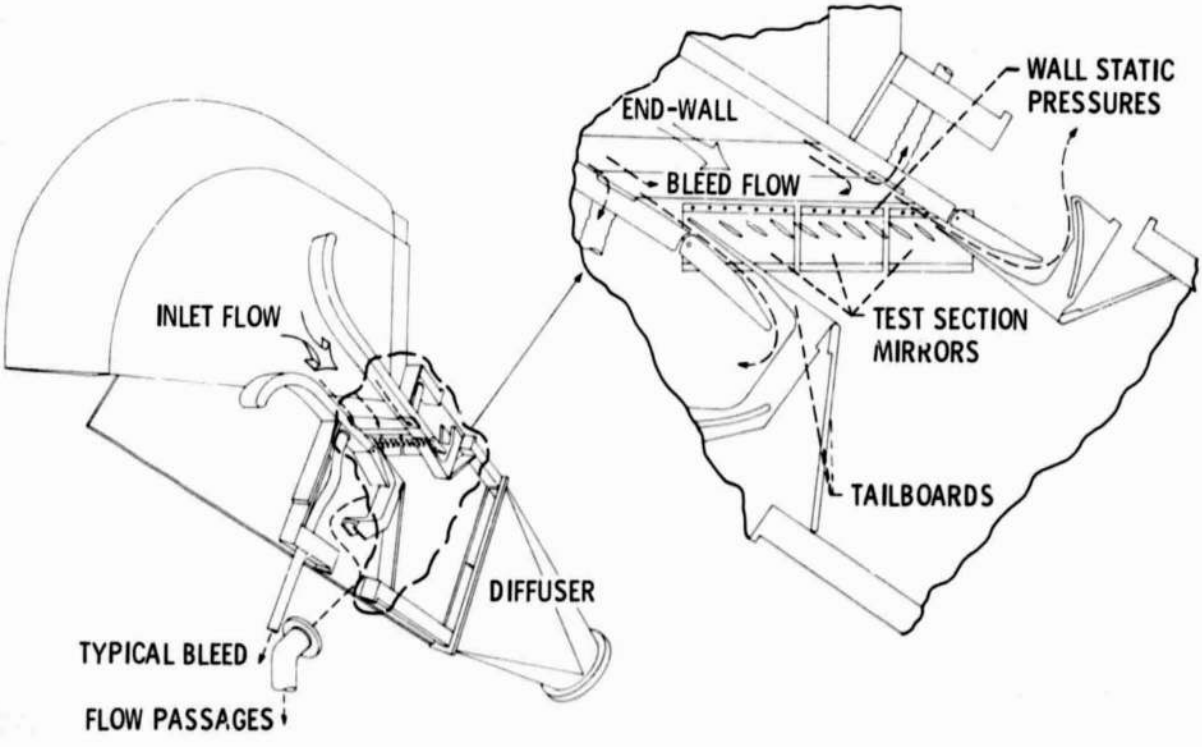

Figure 2. - Test section.

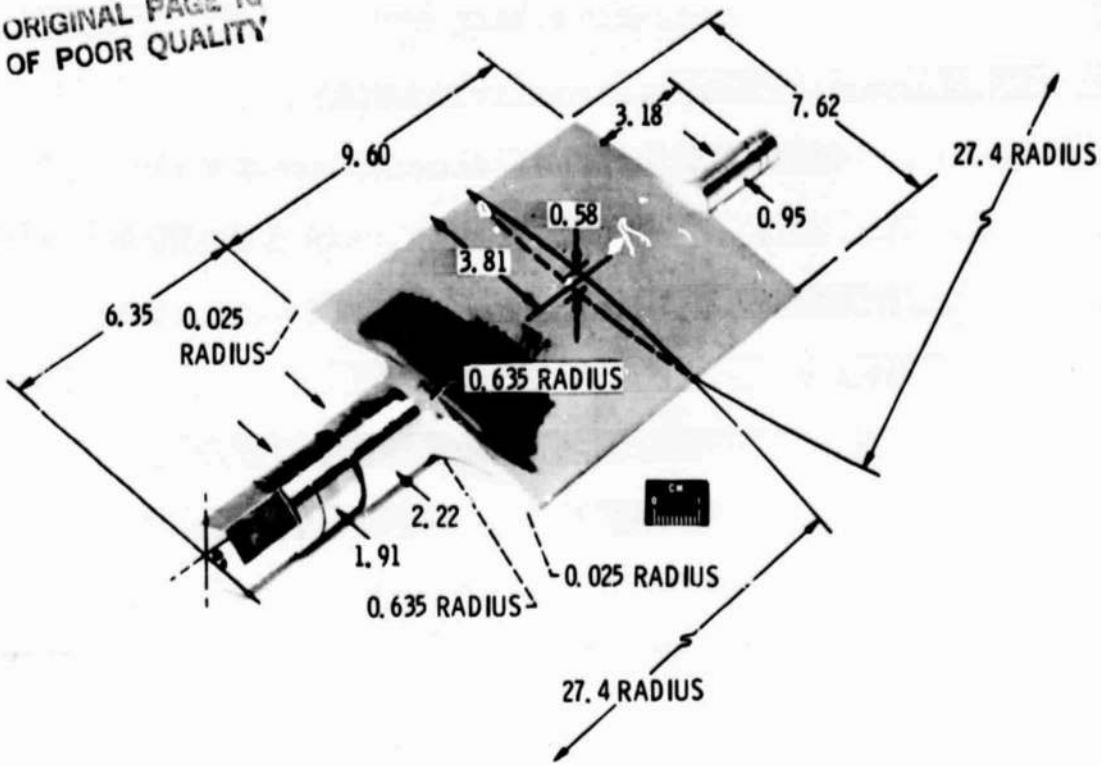

Figure 3. - Biconvex airfoil (all dimensions in centimeters).

SENSOR NUMBER		$\frac{x_c}{C}$
ss	ps	
1	6	0.12
2	5	.25
3	4	.40
4	3	.60
5	2	.75
6	1	.88

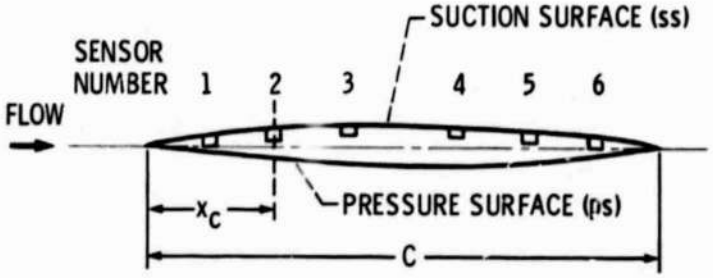

Figure 4. - Location of high-response pressure transducers, C = 7.62 cm.

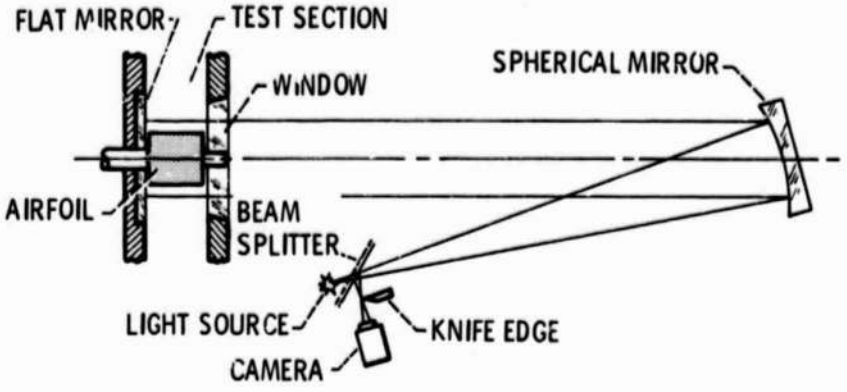

Figure 5. - Double-pass Schlieren system.

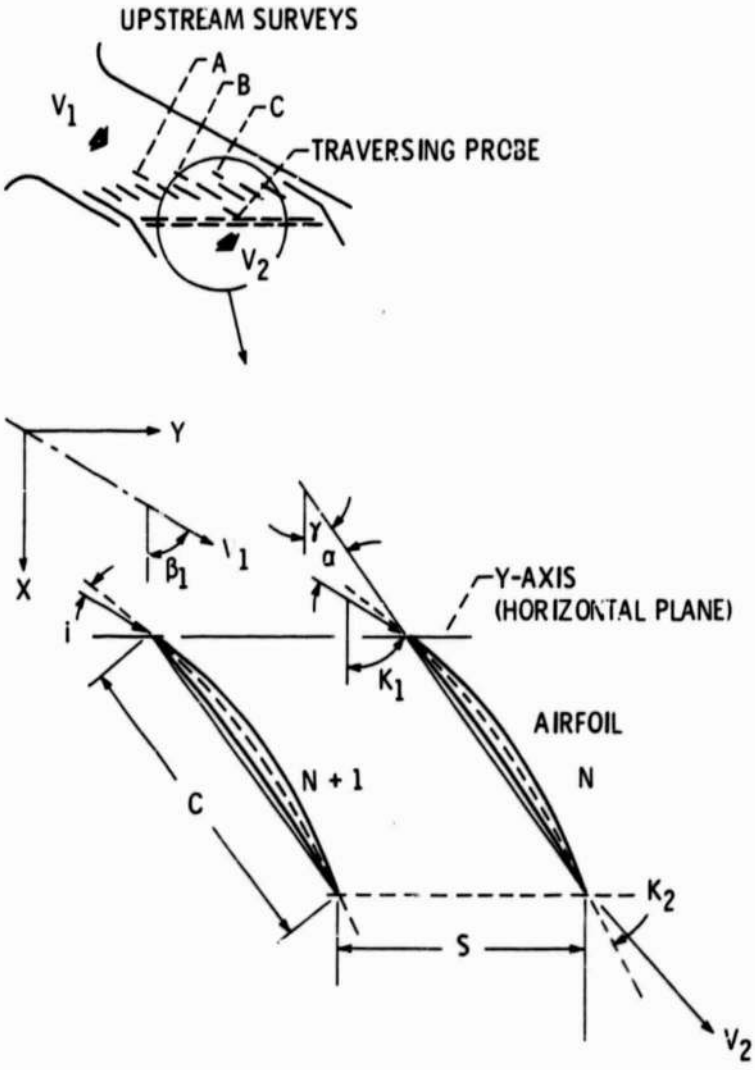

Figure 6. - Coordinate system and geometric parameters.

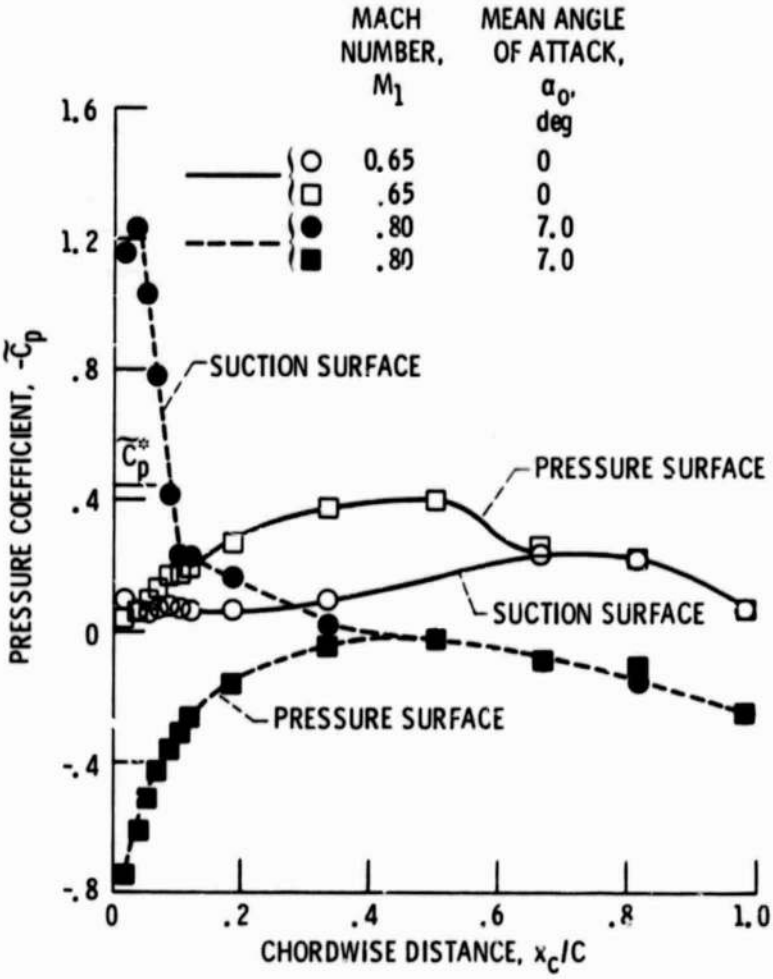

Figure 7. - Steady-state surface pressure distribution on center airfoil.

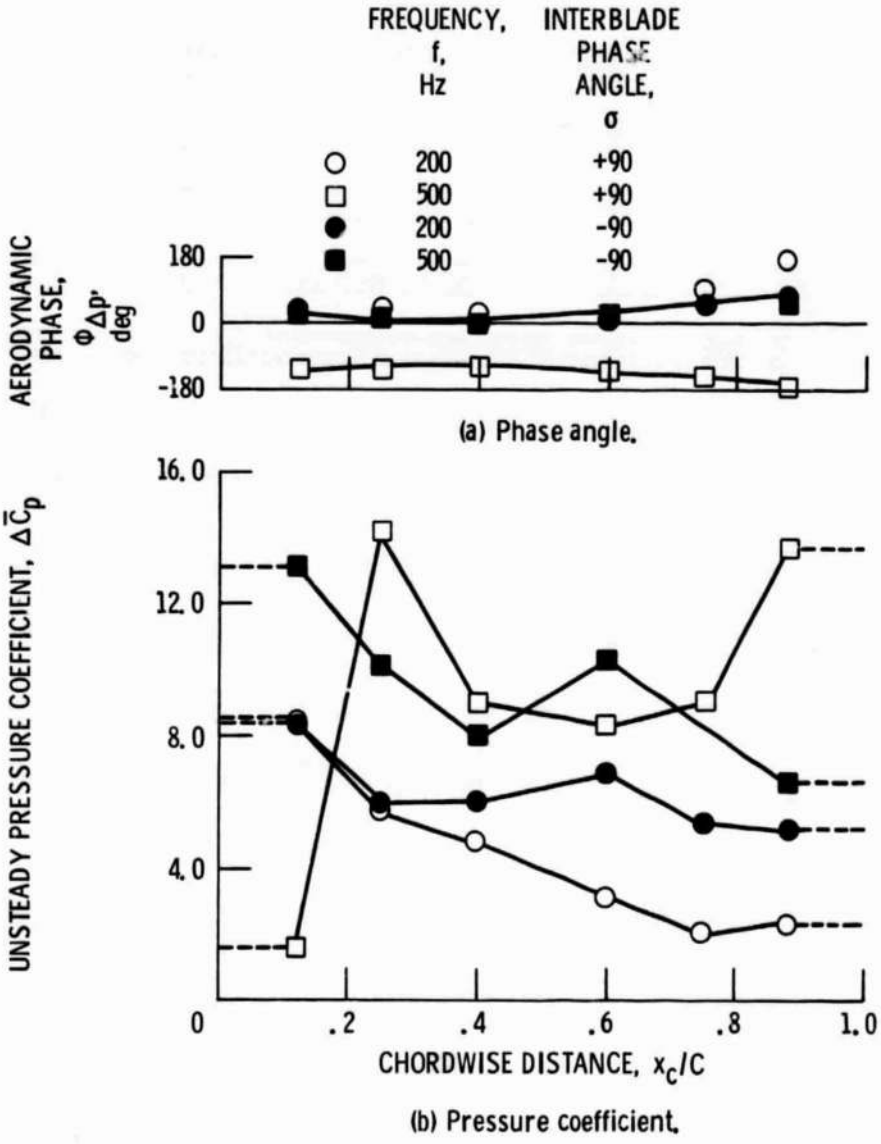

Figure 8. - Distribution of unsteady aerodynamic phase angle and pressure coefficient showing assumed distribution for moment calculation; $M_1 = 0.65$, $\alpha_0 = 0^0$.

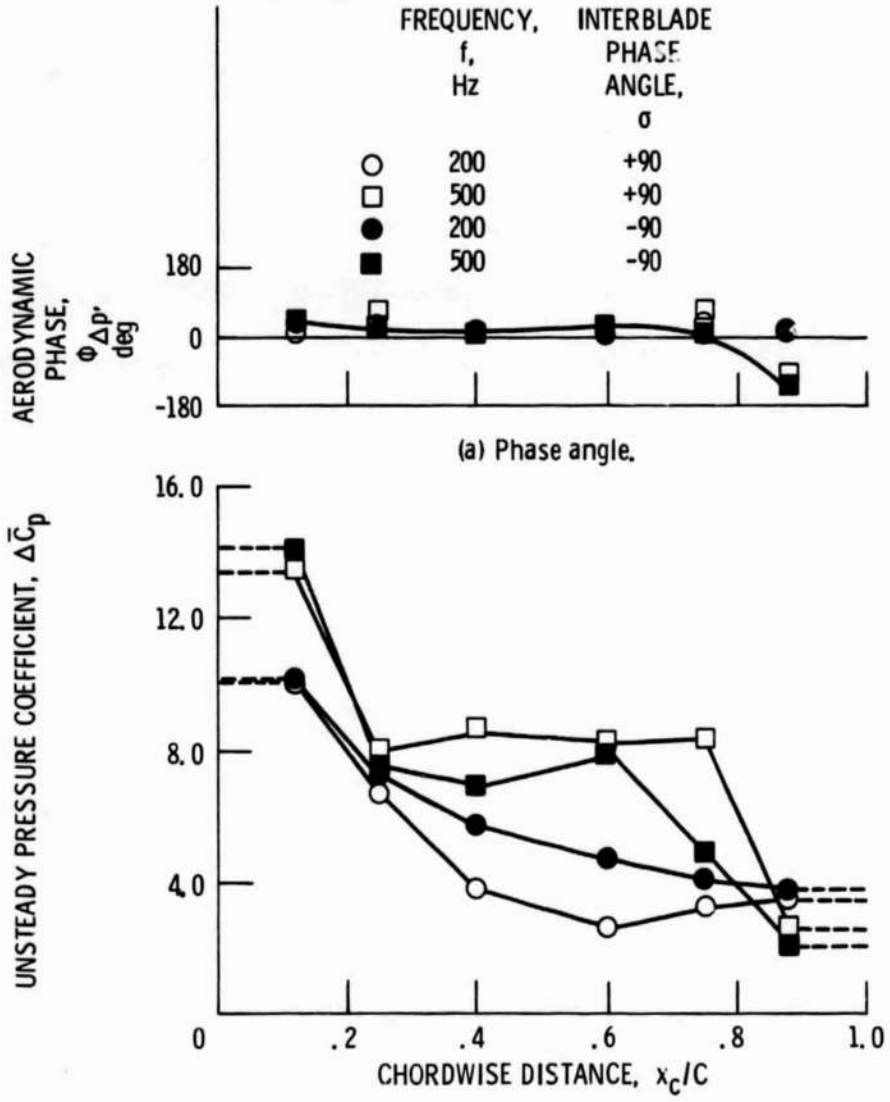

Figure 9. - Distribution of unsteady aerodynamic phase angle and pressure coefficient showing assumed distribution for moment calculation; $M_1 = 0.80$, $\alpha_0 = 7^0$.

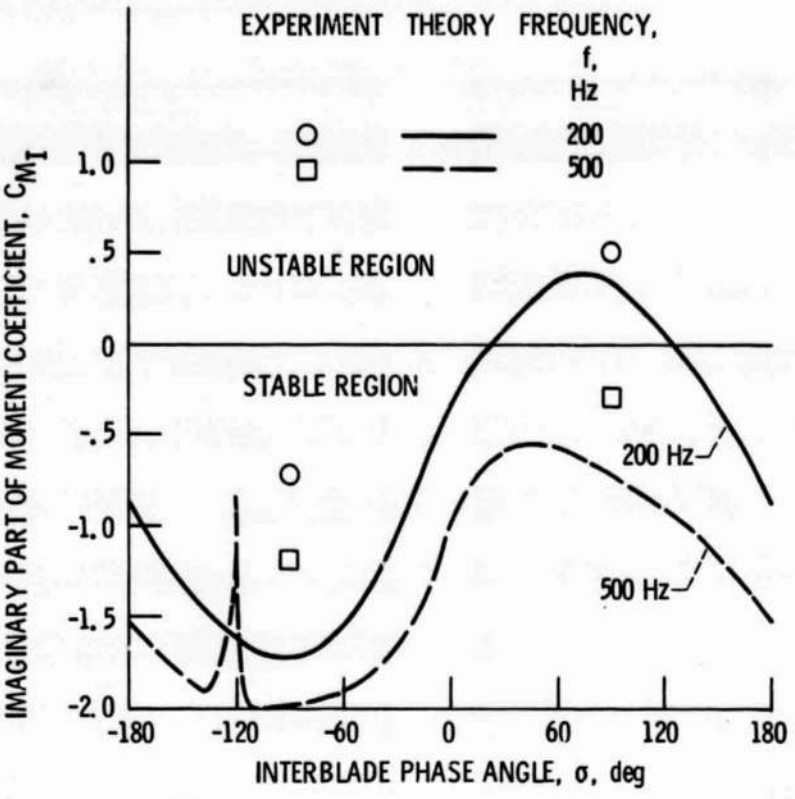

Figure 10. - Comparison of cascade stability results with flat-plate code (9); $M_1 = 0.65$, $\alpha_0 = 0^0$.

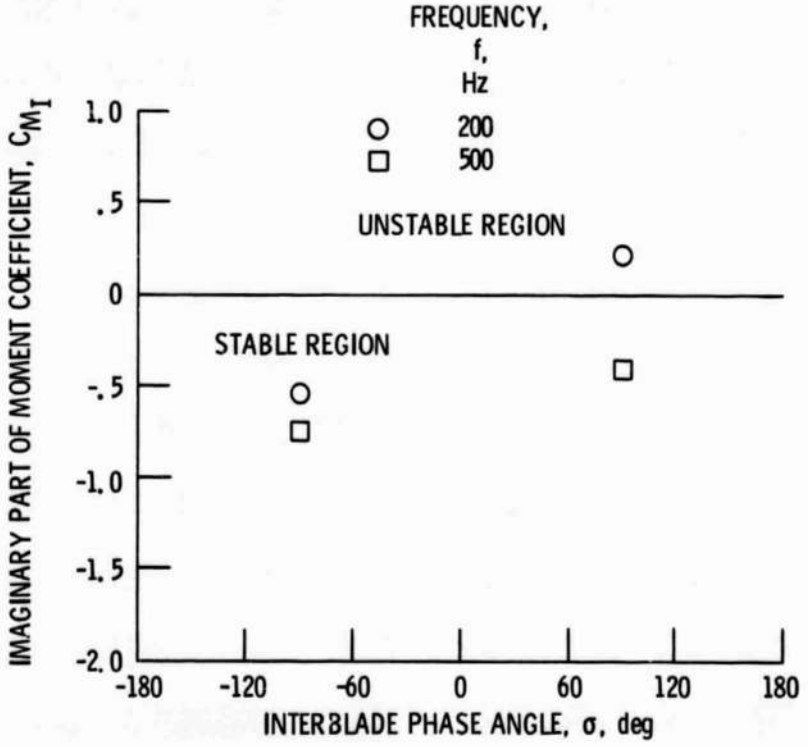

Figure 11. - Experimental stability results; $M_1 = 0.80$, $\alpha_0 = 7^0$.

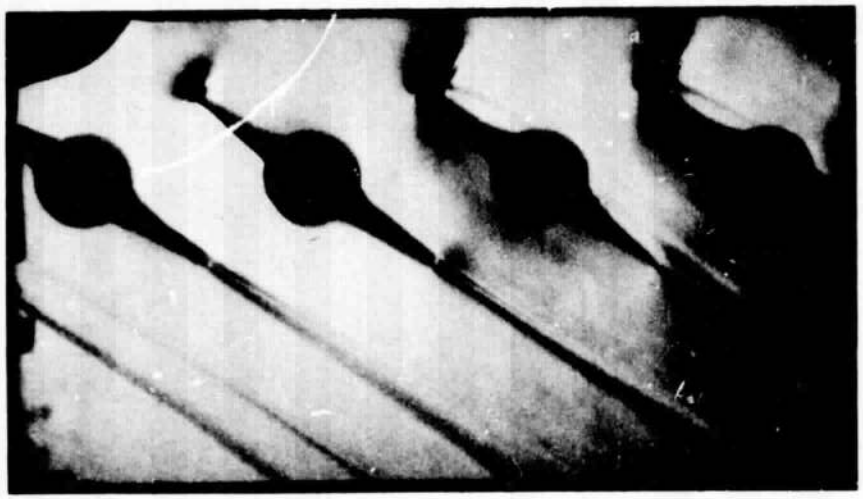

(a) f = 200 Hz, σ = +90 deg.

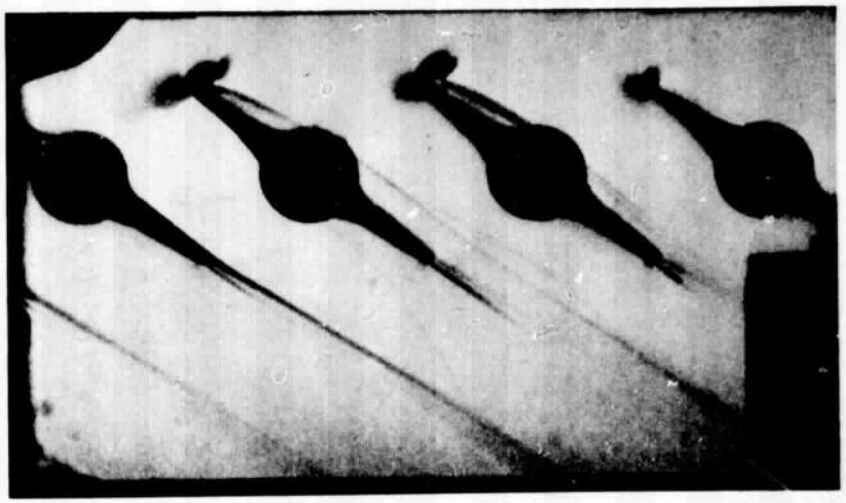

(b) f = 200 Hz, σ = -90 deg.

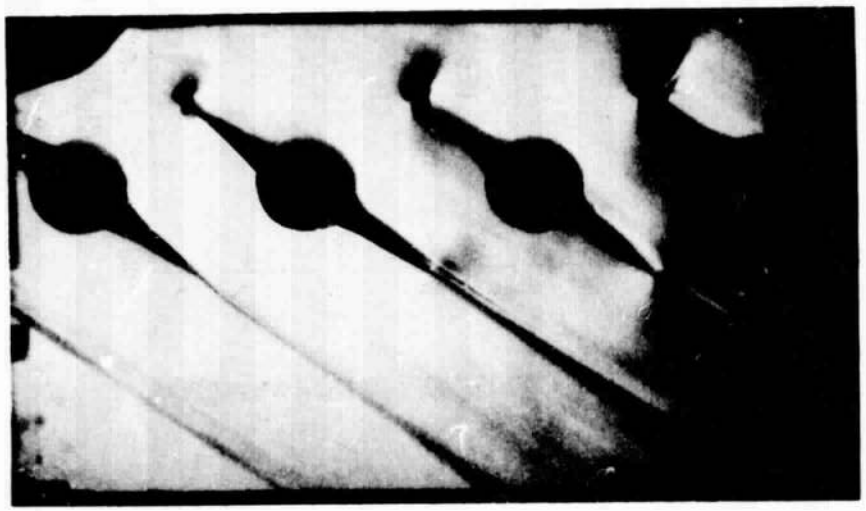

(c) f = 500 Hz, σ = +90 deg.

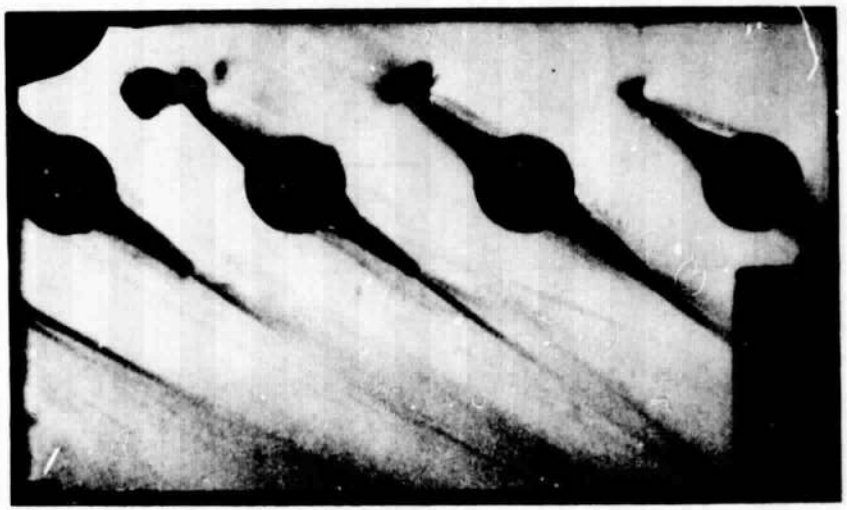

(d) f = 500 Hz, σ = -90 deg.

Figure 12. - Schlieren images of oscillating airfoils at two interblade phase angles and two oscillatory frequencies $M_1 = 0.80$, $\alpha_0 = 7$ deg.